ADVANCED MATERIALS
www.advmat.de

www.MaterialsViews.com

Particle/Fluid Interface Replication as a Means of Producing Topographically Patterned Polydimethylsiloxane Surfaces for Deposition of Lipid Bilayers

By *Anand Bala Subramaniam, Sigolene Lecuyer, Kumaran S. Ramamurthi, Richard Losick,* and *Howard A. Stone**

Microstructured surfaces are common in many materials applications such as microcontact printing,[1,2] biomimetic arrays,[3] controlled-wetting surfaces,[4] superhydrophobic surfaces,[5] and self-cleaning surfaces[6] among others. Most strategies for surface fabrication utilize some form of photolithography to achieve patterning. Photolithographic patterning is essentially two-dimensional;[1–4] it does not allow control over geometric parameters in the third dimension such as the surface profile and curvature (the topography) of fabricated features. To overcome the inherent limitations of photolithography, the fabrication of topographically patterned substrates for applications of supported lipid bilayers[7,8] requires a combination of microfabrication techniques: photolithography followed by anisotropic plasma dry etching and wet oxide etching,[7] or chemical vapor deposition followed by photolithography and chemical etching.[8] These pioneering methods, while successful in producing topographically patterned surfaces capable of imposing gradients of curvature on supported bilayers, are technically complex and require costly cleanroom or microfabrication facilities. An alternative method is thus desirable, particularly since there is intense interest in the role of curvature in the thermodynamics and dynamics of lipid bilayers[7–11] and membrane proteins[12–14] in the wider fields of biology and physics.

Here, we report a method that employs a particle-studded fluid-fluid interface as a template for producing topographically patterned polydimethylsiloxane (PDMS) surfaces with features having positive, negative, and zero mean and Gaussian curvatures. Single or double lipid bilayers that adopt the topography of the underlying substrate can then be deposited onto the plasma-oxidized PDMS surfaces using standard vesicle fusion techniques.[1] Our method has the advantage of not requiring harsh chemicals or cleanroom facilities and is highly versatile. Using this approach we have replicated features of complex geometry such as whole bacterial cells and carbon nanotubes. While the primary goal of our work was to produce solid substrates for applications of supported bilayers, our method can be extended to other systems where a topographically patterned surface is required.

Supported bilayers have been a mainstay of studies utilizing model membranes since they were first reported by Tamm and McConnell.[15] These model systems allow the use of powerful characterization techniques such as fluorescence microscopy,[15] atomic force microscopy (AFM),[16–18] total internal reflection fluorescence microscopy (TIRFM), [17,19,20] and neutron reflectivity,[21] and have been used to study the diffusion of phospholipid molecules,[15] lipid phase separation,[7] lipid raft dynamics,[8] enzyme kinetics,[22] bacterial toxin binding,[20] and have also been used to screen potential drugs.[23] While the majority of supported bilayers are prepared on silica substrates,[7,8,15,17,19] there are reports of bilayers supported on other substrates such as mica,[18] indium tin oxide,[24] titanium dioxide,[24] bare and polymer-covered gold,[16,25] and plasma-oxidized PDMS.[1,23,26,27] Supported bilayers have also been prepared on silica nanoparticles[28] and nanowires,[29] on nanorough substrates such as surface buckled PDMS,[30] silica xerogels,[31] and planar surfaces roughened with adherent nanoparticles.[32] For our goal of topographic patterning, PDMS is the ideal choice since it has a long history as a well-characterized material used to replicate micron to nano-scale structures in the field of soft lithography.[3,4]

The first step towards obtaining a topographically patterned surface is to produce a suitable template off of which the PDMS can be molded. We use a colloidal monolayer at a fluid/fluid interface as our initial template. Note that gel-trapped polystyrene particle monolayers have been used previously to fabricate supraparticles and ''Janus'' particles,[33] and microlens arrays.[34] We believe this method has several advantages: i) Monodisperse colloidal particles of various shapes and sizes are commercially available, or can be synthesized. ii) The curvature of the surface features can be determined a priori by choosing appropriate particles. iii) The whole procedure can be carried out in ambient

[*] Prof. H. A. Stone, A. B. Subramaniam, S. Lecuyer, K. S. Ramamurthi, Prof. R. Losick
Department of Mechanical and Aerospace Engineering
Princeton University
Princeton, NJ 08544
E-mail: hastone@princeton.edu
A. B. Subramaniam, Dr. S. Lecuyer
School of Engineering and Applied Sciences, Harvard University
Cambridge, MA 02138 (USA)
Dr. K. S. Ramamurthi
Laboratory of Molecular Biology, National Cancer Institute Bethesda, MD 20892 (USA)
Prof. R. Losick
Department of Molecular and Cellular Biology, Harvard University
Cambridge, MA 02138 (USA)

DOI: 10.1002/adma.200903625

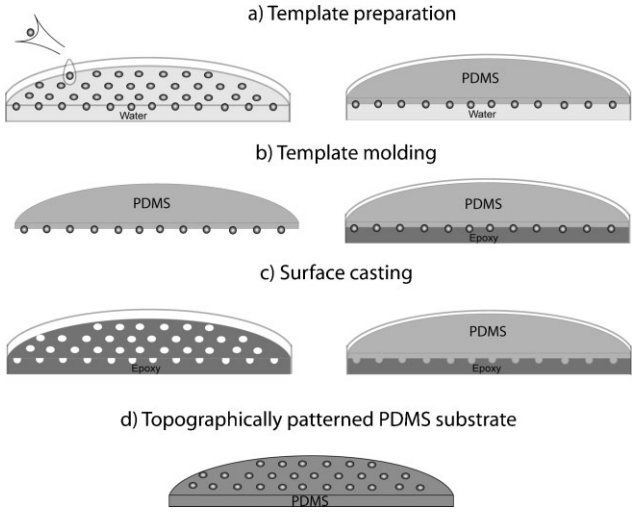

Figure 1. Schematic of the fabrication procedure. a) Colloidal particles are spread on an air-water interface, then PDMS is poured on the surface and cured. b) The colloidal particles are now embedded in the solid PDMS. The surface serves as a template, and a UV-curable epoxy is used to make a mold of the particle-studded surface. To obtain negatively curved features, polystyrene particles are used and are dissolved with DMSO before making the epoxy mold. c) PDMS is poured into the mold and cured to obtain d) an all-PDMS topographically patterned substrate.

laboratory settings with minimal use of harsh chemicals or specialized equipment.

A schematic of our fabrication procedure is outlined in Figure 1. We first discuss how the mean and Gaussian curvatures for spherical features are determined. For a given spherical particle of radius *a,* the mean and Gaussian curvatures are constant over the particle. The two principal curvatures, κ_1 and κ_2, at any point on the particle are equal, that is $\kappa_1 = \kappa_2 = \frac{1}{a}$, so that the mean curvature, $H = \frac{1}{2}(\kappa_1 + \kappa_2) = \frac{1}{a}$ and the Gaussian curvature, $K = \kappa_1\kappa_2 = \frac{1}{a^2}$. Since both definitions of curvature are functions of the particle radius only, the magnitude of the curvature on the final surface features can be chosen by varying the radius of the particles used. Next, we define the direction of the outward normal as pointing away from the surface of the final PDMS substrate. Using this convention, a hemispherical bulge of PDMS has positive mean curvature, and a cavity into the PDMS has negative mean curvature. The sign of the mean curvature of the final features can be chosen by employing the appropriate preparation procedure as we report below.

We start by adding dropwise a dilute suspension of colloidal particles in chloroform onto the surface of a layer of water in a glass petri dish (Fig. 1A). The chloroform spreads on the water surface and evaporates, which leaves the particles trapped at the air-water interface with a well-defined contact angle as revealed previously by gel-trapping[35] and freeze-fracture scanning electron microscopy (SEM).[36] The contact angle of the particles at this stage determines the final feature height, which is an aspect of the fabrication approach that we will return to later.

Next a thin layer of degassed liquid PDMS at a ratio of 9:1 monomer to initiator is poured onto the surface. A wooden applicator stick is used to carefully spread the PDMS over the surface to ensure even coverage. The PDMS floats over the water forming a sharp PDMS-water interface. We found that it is useful for a polystyrene Petri dish cover (or any other suitably flat solid surface) to be floated carefully over the PDMS layer. This step allows the PDMS to harden against a solid surface, which ensures the formation of a thin uniform layer. The PDMS is cured on a hot plate at 65 °C for 2 hours, and then is peeled carefully off of the water surface.

Optical microscopy and SEM images reveal that the silica particles are trapped in the hardened PDMS, which forms a particle-studded surface (see Supporting Information, Figure 1). While it is possible to directly use this studded surface as a substrate to support lipid bilayers, we wished to obtain a surface that only had curvature variations without the potential complication of chemical heterogeneity. Thus, we used a UV-curable epoxy to obtain a mold of the particle-studded surface (Fig. 1B). By casting this (reusable) epoxy mold using fresh PDMS (Fig. 1C) we are able to produce topographically patterned surfaces with features composed entirely of PDMS (Fig. 1D). The use of an epoxy mold also allows surface treatment of the silica particles or the use of non-silica template particles. The mean and Gaussian curvatures on the final PDMS features are positive, while on the flat regions of the surface the mean and Gaussian curvatures are zero.

Features with negative mean curvature can be obtained by substituting the silica particles with uncrosslinked polystyrene particles suspended in ethanol. Once the particle-studded surface is obtained (Fig 1B), we soak the surface in dimethylsulfoxide (DMSO) at 135 °C for 3 hours to dissolve the polystyrene particles. DMSO was chosen since it dissolves polystyrene but not PDMS. The subsequent steps are similar, and we obtain all-PDMS substrates with features that have negative mean curvature, while the Gaussian curvature is positive.

Along with control over the sign and magnitude of the surface curvatures we can also control the height and surface area of the features. The height of the features can be controlled by modifying the wetting characteristics of the template particles. For example, silica particles can be made hydrophobic by grafting hydrocarbon chains onto the silanol surface groups by using alkyl-silanes.[37] A particle that has a large contact angle (more hydrophobic) will have a greater fraction of its surface embedded in the PDMS at the template molding stage and expose a smaller fraction of its curved surface. Thus, for template particles of similar radii, very hydrophobic particles (contact angle $\sim 165^\circ$) result in widely spaced, small spherical caps (Fig. 2A), while less hydrophobic particles (contact angle $\sim 100^\circ$) produce surfaces with smaller interfeature distances, and greater feature height and surface area (Fig. 2B). We emphasize that the mean and Gaussian curvatures of the features are independent of these details and are set only by the radius of the template particles.

The lateral distribution of the features can be modified by changing the number density of particles on the water surface at the template preparation step. Using a low density of particles, we obtain a more disordered distribution of features such as that seen on the surface with negatively curved features in Figure 2C. A higher density of particles results in closer packing and more regular ordering of the features.[34,35,37]

One natural consequence of our method is that we can obtain surfaces with features of positive, negative, and zero mean curvatures that are adjacent and connected. One such surface is shown in Figure 2D. A supported bilayer on this substrate will

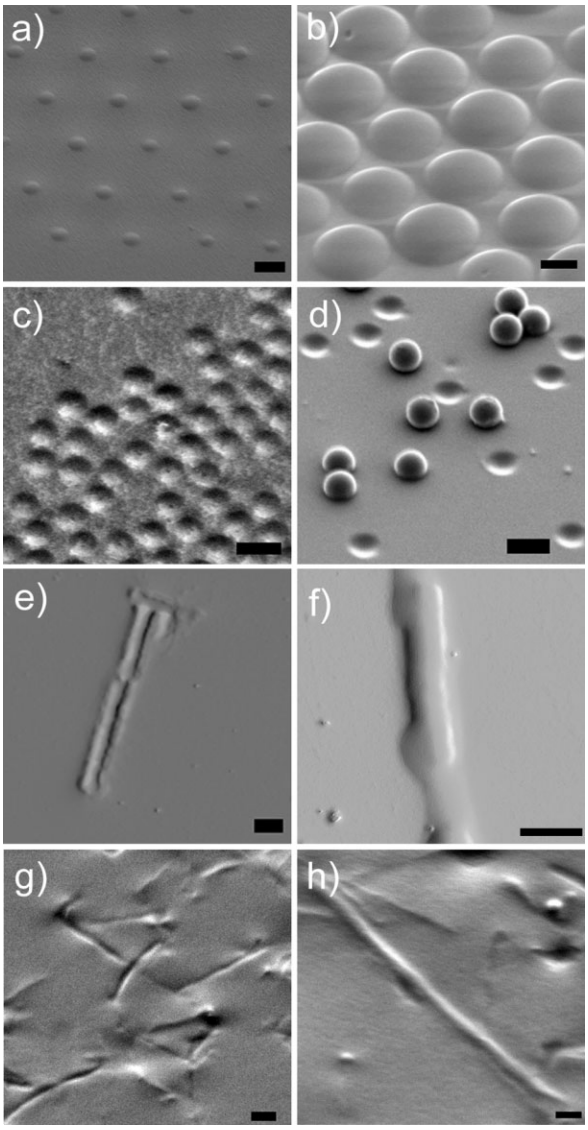

Figure 2. Examples of topographically patterned PDMS substrates. a–d,g,h) SEM images. a,b) Both surfaces fabricated with 2.37 μm radius silica particles as template particles. Silica particles in (a) were treated with chloro(dodecyl)dimethylsilane, which makes them very hydrophobic (contact angle 165°). Template particles in (b) were treated with chlorotrimethysilane. The shorter carbon chain produces a less hydrophobic particle, which leads to a smaller contact angle and thus larger feature height. Features on both surfaces have the same mean and Gaussian curvatures, which are set by the radius of the template particle. c) Features with negative mean curvature and positive Gaussian curvature fabricated using 800 nm radius polystyrene particles. d) Surface with features of both positive and negative mean curvatures. The planar regions in between the features have zero mean curvature. Thus all three possible signs of curvature are present on this surface. e,f) AFM amplitude trace of surfaces fabricated with rod-shaped bacterial cells as template particles e) Surface with negative mean curvature features, which are replicas of *B.subtilis*. f) A zoomed in scan of a positive mean curvature replica of *B.subtilis*. Unidentified extracellular material is also reproduced by the casting process. The sign of the Gaussian curvature changes along the shape as discussed in the text. g) Surfaces with negative mean curvature cylindrical features fabricated by replicating multi-walled carbon nanotubes h) Positive mean curvature cylindrical features, which are replicas of carbon nanotubes. a–d) Scale bar 2 μm, e,f,g) scale bar 1 μm, h) scale bar 500 nm.

have all three possible signs of curvature, which is a property that cannot be achieved easily with liposomal systems. Another advantage of the technique is that it is relatively straightforward to produce surface features with exotic geometries by using non-spherical particles such as ellipsoids,[38] microrods,[39] carbon nanotubes, or even biological particles. As an example of the latter, we used the rod-shaped bacteria *Bacillus subtilis* as our template particle to produce both negative (Fig. 2E) and positive (Fig. 2F) replicas of the bacterial cell wall. We suggest that bilayers supported on these features may be the closest in vitro mimic of the actual geometry of the bacterial plasma membrane. We note that unlike spherical particles, the geometry of these rod-shaped particles is non-trivial: the magnitude of the mean and Gaussian curvatures varies over the feature. In the idealized case of the bacterial particle modeled as a spherocylinder, the Gaussian curvature is positive for the spherical endcaps (bacterial poles), and zero for the cylindrical body, while the magnitude of the mean curvature is twice as large on the poles compared to the body. Surfaces decorated with small and highly curved features can be fabricated by replicating nanomaterials such as multi-walled carbon nanotubes. The surfaces with negative and positive replicas of carbon nanotubes shown in Figure 2G and 2H respectively have radii of curvatures ~50–150 nm.

To illustrate the possibilities of these surfaces for studies of membrane biophysics, we prepared DOPC single bilayers labeled with 0.5 mole percent of the fluorescent lipid probe rhodamine-DPPE on surfaces with spherical-shaped and bacterial-shaped features. Lipid bilayers are imaged in confocal fluorescence mode while the underlying topographically patterned substrates are imaged in transmission mode. The three-dimensional confocal slices are projected as a two-dimensional image using the 'sum slices' method, and an orthogonal view through the bilayer supported on the substrate with spherical features is shown (Fig. 3).

In the absence of large defects, fluorescently labeled DOPC bilayers on planar substrates are known to be homogenous.[1,26] On our topographically patterned substrates, the large difference in length scales between the thickness of the bilayer (~5 nm[28]) and the radius of curvature of the surface features (~1000 nm) suggests that the distribution of lipids should be similar to that on a planar substrate. Thus, we expect that the fluorescence intensity in the two-dimensional projections to be insensitive to the underlying curved features. Indeed, we observe a uniformly fluorescent bilayer adsorbed on both the surface with the spherical features (Fig. 3B) and the more geometrically complex bacterial-shaped features (Fig. 3D). A line intensity profile through the flat and curved regions of the bilayer supported on the surface with the spherical features confirms the absence of correlation between the bilayer fluorescence intensity (Fig. 3F) and the position of the curved features (Fig. 3E). Note however, that the topographical patterning is apparent in the orthogonal slice through the bilayer (Fig. 3F inset). We thus conclude, within the resolution limit of the confocal microscope, that our PDMS substrates support homogenous topographically patterned bilayers with no apparent defects.

To test for the presence of bilayer defects below the resolution limit of the confocal microscope, we probe lipid diffusion in the topographically patterned bilayers through fluorescence recovery after photobleaching (FRAP) measurements. High quality DOPC

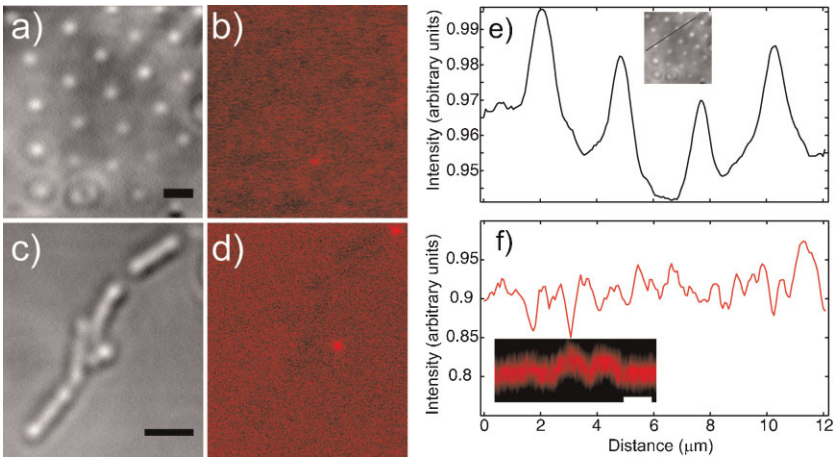

Figure 3. Confocal images of lipid bilayer covered substrates. a) Transmitted light image of 1.28 μm radius positively curved features. b) Z-projection using the sum slices method. c) Transmitted light image of *B. subtilis* features d) Z-projection using the sum slices method, intensity is uniform throughout the bilayer except for bright points where unfused small vesicles remain adsorbed to the bilayer. Normalized line intensity profile for the spherical features (inset shows line chosen) through: e) the transmitted light image, where the centers of the features appear as intensity maxima. f) rhodamine-DPPE labeled bilayer, showing, as expected, that bilayer fluorescence intensity does not correlate with the position of the underlying features. An orthogonal section through the bilayer demonstrates the topographical patterning. Scale bars 2 μm.

bilayers with minimal defects have laterally mobile lipids with a diffusion coefficient $O(10^{-8})$ cm^2s^{-1}.[1,26] We again use surfaces decorated with spherical features of 1.28 μm radius of curvature with the expectation that the small curvature of the features will have a negligible impact on lipid diffusion. Thus, we should obtain similar diffusion coefficients on the curved and flat regions of the supported bilayer. We measure a lipid diffusion coefficient of $(1.8 \pm 0.2) \times 10^{-8}\,cm^2\,s^{-1}$ on the curved features and $(1.7 \pm 0.1) \times 10^{-8}\,cm^2\,s^{-1}$ on the flat regions of the substrate. These values are comparable to those reported in the literature for lipid diffusion coefficients on non-patterned glass and PDMS,[1,26] and confirm that the lipids in the bilayer diffuse freely along the topography of the patterned surface.

Finally, we demonstrate that double bilayers supported on our topographically patterned PDMS surfaces reproduce curvature-modulated phase separation observed on double bilayers supported on microfabricated silica substrates. It is known that DPPC/DOPC/cholesterol ternary mixtures phase separate into coexisting liquid-ordered (L_o) and liquid-disordered (L_d) phases below a miscibility transition temperature, and that the fluorescent lipid probe rhodamine-DPPE partitions to the L_d phase.[40] On microfabricated silica substrates L_d domains align along features of higher curvature.[7] Similar to Parthasarathy et al.,[7] we first deposit a lower bilayer labeled with the fluorescent lipid probe NBD-PC through the vesicle fusion technique. We then rupture giant unilamellar vesicles onto the lower bilayer to form well-defined double bilayer patches. A double bilayer is necessary to decouple the upper membrane from the strong influence of the solid substrate on lipid phase behavior.[7] Since the upper bilayers are below the miscibility transition temperature the lipids phase separate into bright L_d domains (Fig. 4A), which are seen as intensity peaks in the line intensity profile (Fig. 4E), against a darker L_o background. The line intensity profile through the lower bilayer (Fig. 4B) reveals that local maxima in rhodamine intensity correlate with local minima in NBD fluorescence (Fig. 4F). This drop in NBD fluorescence intensity can be explained by the non-radiative Förster resonance energy transfer (FRET) between the NBD from the lower bilayer to the rhodamine containing domains in the upper bilayer.[7] The transmitted light

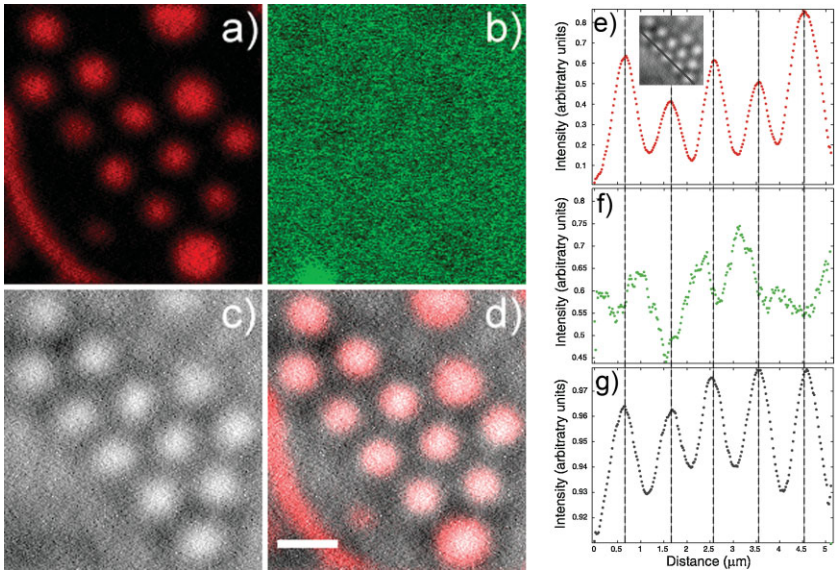

Figure 4. Curvature-modulated phase separation in a supported lipid bilayer, demonstrated on a PDMS substrate with positively curved features with radius of curvature of 500 nm: a) Fluorescence image of the upper bilayer composed of DPPC/DOPC/cholesterol/DOTAP mixture labeled with 0.5 mol percent rhodamine-DPPE, below the miscibility transition temperature. The rhodamine-DPPE segregates to the cholesterol poor L_d phase which appears as bright domains while the cholesterol rich L_o phase appears dark. The edge of the bilayer patch can be seen as the curved line at bottom left of the image. b) Fluorescence image of the lower DMPC/NBD-PC bilayer. c) Transmitted light image of the underlying substrate d) Superimposed image of the upper bilayer and the transmitted light image. Scale bar 1 μm. e–f) Normalized line intensity profile (inset shows line chosen) through: e) Upper bilayer. f) Lower bilayer. Maxima in rhodamine intensity corresponds to a minima in NBD intensity, due to Förster resonance energy transfer (FRET) between the NBD from the lower bilayer and the rhodamine in the upper bilayer [7]. g) Transmitted light image of the substrate. The centers of the features appear as intensity maxima. The vertical lines are guides to the eye showing that maxima in upper bilayer intensity correspond to the centers of the curved features. It is clear that the L_d phase preferentially localizes to the positively curved features.

image of the underlying substrate (Fig. 4C) and the corresponding line intensity profile (Fig. 4G) demonstrate that the L_d phase preferentially localizes to regions of higher curvature and also to the edges of the upper bilayer patch. Clearly our all-PDMS topographically patterned surface reproduces the results reported for patterned silica substrates.

In conclusion, we have reported a method for producing topographically patterned PDMS substrates by replicating a particle-studded fluid/fluid interface. This method is simpler than current fabrication protocols and produces surfaces decorated with features of well-defined curvature gradients and geometry. We have shown that these substrates support high quality lipid bilayers and confirm that the substrates reproduce previously reported results on curvature-modulated phase separation of lipid bilayers. Looking forward, it is clear that this system could be used to test the curvature sensitivity of a variety of membrane associated proteins, particularly bacterial proteins that are reported to be sensitive to positive or negative curvatures on the order of 500 nm^{-1}. Indeed, the bacterial shaped surfaces we have shown might be an excellent in vitro system to address the vexing question of pole localization observed for many proteins[12,14] and plasma membrane lipid components[11] in bacteria.

Experimental

Chemicals and Particles: Dry monodisperse silica particles of radii 270 nm, 500 nm, 1.28 μm, and 2.37 μm were purchased from Bangs Labs. Surfactant-free monodisperse polystyrene particles of radii 750 and 800 nm were purchased from Invitrogen. Multi-walled carbon nanotubes (O.D. × L = 110–170 nm × 5–9 μm, >90% carbon basis). Dimethylsulfoxide (DMSO) (purity 99.9%), chlorotrimethylsilane (purity 99.0%), and chloro(dodecyl)dimethylsilane (purity > 95.0%) were all purchased from Sigma. Sylgard 184 was purchased from Dow Corning and Epotek UVO-118 UV-curable epoxy was purchased from Epoxy Technology. 1,2-dimyristoyl-*sn*-glycero-3-phosphocholine (DMPC), 1,2-dioleoyl-*sn*-glycero-3-phosphocholine (DOPC), 1,2-dioleoyl-3-trimethylammonium-propane (chloride salt) (DOTAP), 1,2-dipalmitoyl-*sn*-glycero-3-phosphoethanolamine-*N*-(lissamine rhodamine B sulfonyl) (ammonium salt) (rhodamine-DPPE), 1-oleoyl-2-[12-[(7-nitro-2-1,3-benzoxadiazol-4-yl)amino] lauroyl]-*sn*-Glycero-3-phosphocholine (NBD-PC), 1,2-dipalmitoyl-*sn*-glycero-3-phosphocholine (DPPC), cholesterol (ovine wool) were all purchased from Avanti Polar Lipids.

Lipid Compositions: Figure 3, DOPC/rhodamine-DPPE 99.5/0.5 mole percent, FRAP measurements, DOPC/NBD-PC 99/1 mole percent, Figure 4, lower bilayers DMPC/NBD-PC 97/3 mole percent, upper bilayers DPPC/DOPC/Cholesterol/DOTAP/rhodamine-DPPE 53.5/25/20/1.5/0.5 mole percent. Supported bilayers were prepared using standard vesicle fusion techniques [1,7,8,26]. See the Supporting Information for further details.

Substrate Imaging: Scanning electron microscope (SEM) images were obtained using a Zeiss Supra55 FESEM. The PDMS substrates were sputter-coated with gold prior to imaging. AFM images of bacterial replicas were obtained with an Asylum MFP 3D AFM in tapping mode. Supported lipid bilayers were imaged with an upright confocal microscope (Zeiss LSM 510) with a 63x/ 1.0 N.A. water dipping objective.

Image Processing and FRAP Measurements: Horizontal scanning artifacts in the transmitted light images were removed in ImageJ through FFT filtering. The Z-projections in Figure 3 and line intensity profiles in Figures 3 and 4 were obtained in ImageJ. Raw intensity data was normalized by setting the maximum intensity for each channel to 1. Normalized intensity data was then smoothed in Matlab (version 7.8) using the moving average method with a span of 5. FRAP was done with the 488 nm laser line of an argon laser, bleaching was carried out at 100 percent laser power, and imaging of the subsequent recovery was carried out with the laser at 0.1% intensity. Experiments were repeated 20 times each over different areas on both the flat and curved regions. Raw region of interest intensity data were normalized by setting pre-bleach intensities to 1 and first post-bleach intensity to zero. The normalized recovery curves were fitted in Matlab using a single exponential model (nonlinear least squares).

Acknowledgements

We thank the Harvard MRSEC (DMR-0820484) and the Harvard Center for Brain Science Imaging Facility. We also thank Dr. J.D. Deng for help with AFM imaging. Supporting Information is available online from Wiley InterScience or from the authors.

Received: October 22, 2009
Published online: April 7, 2010

[1] J. S. Hovis, S. G. Boxer, *Langmuir* **2001**, *17*, 3400.
[2] Y. N. Xia, G. M. Whitesides, *Annu. Rev. Mater. Sci.* **1998**, *28*, 153.
[3] B. Pokroy, A. K. Epstein, M. C. M. Persson-Gulda, J. Aizenberg, *Adv. Mater.* **2009**, *21*, 463.
[4] L. Courbin, E. Denieul, E. Dressaire, M. Roper, A. Ajdari, H. A. Stone, *Nat. Mater.* **2007**, *6*, 661.
[5] D. Oner, T. J. McCarthy, *Langmuir* **2000**, *16*, 7777.
[6] R. Blossey, *Nat. Mater.* **2003**, *2*, 301.
[7] R. Parthasarathy, C.-h. Yu, J. T. Groves, *Langmuir* **2006**, *22*, 5095.
[8] T.-Y. Yoon, C. Jeong, S.-W. Lee, J. H. Kim, M. C. Choi, S.-J. Kim, M. W. Kim, S.-D. Lee, *Nat. Mater.* **2006**, *5*, 281.
[9] A. Tian, T. Baumgart, *Biophys. J.* **2009**, *96*, 2676.
[10] B. Sorre, A. Callan-Jones, J.-B. Manneville, P. Nassoy, J.-F. o. Joanny, J. Prost, B. Goud, P. Bassereau, *Proc. Natl. Acad. Sci. USA* **2009**, *106*, 5622.
[11] K. C. Huang, R. Mukhopadhyay, N. S. Wingreen, *PLoS Comput. Biol.* **2006**, *2*, 1357.
[12] K. S. Ramamurthi, R. Losick, *Proc. Natl. Acad. Sci. USA* **2009**, *106*, 13541.
[13] K. S. Ramamurthi, S. Lecuyer, H. A. Stone, R. Losick, *Science* **2009**, *323*, 1354.
[14] R. Lenarcic, S. Halbedel, L. Visser, M. Shaw, L. J. Wu, J. Errington, D. Marenduzzo, L. W. Hamoen, *EMBO J.* **2009**, *28*, 2272.
[15] L. K. Tamm, H. M. McConnell, *Biophys. J.* **1985**, *47*, 105.
[16] M. Li, M. Chen, E. Sheepwash, C. L. Brosseau, H. Li, B. Pettinger, H. Gruler, J. Lipkowski, *Langmuir* **2008**, *24*, 10313.
[17] S. W. Hui, R. Viswanathan, J. A. Zasadzinski, J. N. Israelachvili, *Biophys. J.* **1995**, *68*, 171.
[18] S. Singh, D. J. Keller, *Biophys. J.* **1991**, *60*, 1401.
[19] E. Sackmann, *Science* **1996**, *271*, 43.
[20] J. M. Moran-Mirabal, J. B. Edel, G. D. Meyer, D. Throckmorton, A. K. Singh, H. G. Craighead, *Biophys. J.* **2005**, *89*, 296.
[21] S. Lecuyer, G. Fragneto, T. Charitat, *Eur. Phys. J. E* **2006**, *21*, 153.
[22] M. Grandbois, H. Clausen-Schaumann, H. Gaub, *Biophys. J.* **1998**, *74*, 2398.
[23] T. Yang, S-. y. Jung, H. Mao, P. S. Cremer, *Anal. Chem.* **2000**, *73*, 165.
[24] C. Merz, W. Knoll, M. Textor, E. Reimhult, *Biointerphases* **2008**, *3*, FA41.
[25] L. Zhang, M. L. Longo, P. Stroeve, *Langmuir* **2000**, *16*, 5093.
[26] K. S. Phillips, Q. Cheng, *Anal. Chem.* **2004**, *77*, 327.
[27] T. Shahal, K. A. Melzak, C. R. Lowe, E. Gizeli, *Langmuir* **2008**, *24*, 11268.
[28] S. Mornet, O. Lambert, E. Duguet, A. Brisson, *Nano Lett.* **2005**, *5*, 281.
[29] S. C. J. Huang, A. B. Artyukhin, J. A. Martinez, D. J. Sirbuly, Y. Wang, J. W. Ju, P. Stroeve, A. Noy, *Nano Lett.* **2007**, *7*, 3355.
[30] B. Sanii, A. M. Smith, R. Butti, A. M. Brozell, A. N. Parikh, *Nano Lett.* **2008**, *8*, 866.
[31] E. I. Goksu, B. A. Nellis, W.-C. Lin, J. H. Satcher, Jr, J. T. Groves, S. H. Risbud, M. L. Longo, *Langmuir* **2009**, *25*, 3713.

[32] Y. Roiter, M. Ornatska, A. R. Rammohan, J. Balakrishnan, D. R. Heine, S. Minko, *Langmuir* **2009**, *25*, 6287.
[33] V. N. Paunov, O. J. Cayre, *Adv. Mater.* **2004**, *16*, 788.
[34] O. J. Cayre, V. N. Paunov, *J. Mater. Chem.* **2004**, *14*, 3300.
[35] O. J. Cayre, V. N. Paunov, *Langmuir* **2004**, *20*, 9594.
[36] A. B. Subramaniam, M. Abkarian, L. Mahadevan, H. A. Stone, *Langmuir* **2006**, *22*, 10204.
[37] T. S. Horozov, R. Aveyard, J. H. Clint, B. P. Binks, *Langmuir* **2003**, *19*, 2822.
[38] C. C. Ho, R. H. Ottewill, A. Keller, J. A. Odell, *Polym. Int.* **1993**, *30*, 207.
[39] R. G. Alargova, D. S. Warhadpande, V. N. Paunov, O. D. Velev, *Langmuir* **2004**, *20*, 10371.
[40] T. S. Ursell, W. S. Klug, R. Phillips, *Proc. Natl. Acad. Sci. USA* **2009**, *106*, 13301.